Photoinitiation mechanisms of novel phenothiazine-based oxime and oxime esters acting as visible light sensitive Type I and multicomponent photoinitiators

Adel Noon, Fatima Hammoud, Bernadette Graff, Tayssir Hamieh, Joumana Toufaily, Fabrice Morlet-Savary, Michael Schmitt, Thanh-tuan Bui, Alexandre Rico, Fabrice Goubard, et al.

Photoinitiation mechanisms of novel phenothiazine-based oxime and oxime esters acting as visible light sensitive Type I and multicomponent photoinitiators

Adel Noon[1,2,3], Fatima Hammoud[1,2], Bernadette Graff[1,2], Tayssir Hamieh[3], Joumana Toufaily[3], Fabrice Morlet-Savary[1,2], Michael Schmitt[1,2], Thanh-Tuan Bui[4*], Alexandre Rico[5], Fabrice Goubard[4], Sébastien Péralta[4], Frédéric Dumur[4,5,6*], Jacques Lalevée[1,2*]

[1] Université de Haute-Alsace, CNRS, IS2M UMR 7361, F-68100 Mulhouse, France.
[2] Université de Strasbourg, Strasbourg, France.
[3] Laboratory of Materials, Catalysis, Environment and Analytical Methods (MCEMA), Faculty of Sciences, Doctoral School of Sciences and Technology (EDST), Lebanese University, Beirut 6573-14, Lebanon.
[4] CY Cergy Paris Université, LPPI, F-95000 Cergy, France.
[5] Aix Marseille Univ, CNRS, ICR UMR 7273, F-13397 Marseille, France.
[6] CY Cergy Paris Université, CY Advanced Studies, F-95000 Cergy, France.
*Corresponding authors: tbuy@cyu.fr; frederic.dumur@univ-amu.fr; jacques.lalevee@uha.fr

Abstract:

In this work, three new photoinitiators, based on the phenothiazine scaffold as a chromophore and potentially bearing the oxime ester functionality as an initiating group were designed and synthesized for the free radical polymerization of acrylates, the cationic polymerization of epoxides, and the formation of interpenetrated polymer networks upon irradiation with a light emitting diode emitting at 405 nm. These phenothiazine-based oxime and oxime esters revealed impressive photoinitiation ability manifested by excellent polymerization rates and high final reactive function conversions. Significantly, they can be used as both; one-component (Type I) and two-component photoinitiating systems. Photoinitiation mechanisms through which reactive species are produced were investigated by means of different complementary techniques including real-time Fourier transform infrared spectroscopy, UV-visible absorption spectroscopy, electron spin resonance spectroscopy, fluorescence (steady state and time resolved), cyclic voltammetry, and molecular modelling calculations. Thermal initiation behavior of the different oxime esters was also studied by using differential scanning calorimetry, highlighting their dual

thermal/photochemical initiation ability. Finally, 3D printed objects were successfully fabricated by conducting both direct laser write and 3D printing experiments.

Keywords: Photoinitiators, visible range, LEDs, Oxime esters, Thermal initiators, 3D printing

1. Introduction

In recent years, light-induced polymerization processes have gained an accelerative attention due to their environmental advantages over other industrial processes. It proceeds with low or no volatile organic compounds emissions, low energy consumption, and excellent time and spatial control.[1,2] Consequently, this polymerization technique has been extensively used in numerous applications including adhesives, coatings, dental materials, biomaterials, 3D printing, optics, microelectronics, and nanotechnology etc.[3-5] Nowadays, light-emitting diodes (LEDs) appeared to be significant alternatives to the traditional UV irradiation sources (e.g. Hg lamps). Notably, LEDs can compete with these traditional light sources due to numerous advantages such as low operating costs, faster switching times, low energy consumption, low heat generation, longer emission wavelengths, portability, simplicity, easy availability and safety in handling.[6-8] The initiation step for free radical polymerization (FRP) of acrylate function or cationic polymerization (CP) of epoxy function depends on the utilized photoinitiator (PI) which constitutes the key-component of the resin in charge to generate active species under light irradiation. Therefore, one of the most important challenges is the development of new PIs for both FRP and CP with absorption properties that are in complement with the emission wavelength of the LEDs.[9, 10]

In order to overcome the drawbacks of two-component photoinitiating systems (or even more generally for multicomponent systems) which are easily influenced by the electron transfer efficiency, the viscosity and the polarity of the resin,[11-13] it is advantageous to develop unimolecular photoinitiating systems (Type I PIs) where these diffusion controlled influences do not exist.[14] However, most of the Type I PIs absorb the irradiation only in the UV range and only few PIs such as amino acetophenones (e.g. Irgacure 369) and phosphine oxides (e.g. TPO, TPO-L and BAPO) can be activated upon excitation at 405 nm. In this context, oxime esters (OXEs) are considered as highly-efficient Type I PIs[15, 16] as OXEs can undergo a homolytic cleavage of the N-O bond under light irradiation, enabling to generate iminyl and acyloxy free radicals. The latter can decarboxylate

and produce active species along with the generation of CO_2[17]. Especially, in these structures, the decarboxylation step is a key parameter avoiding radical recombination. Indeed, due to the decarboxylation reaction, alkyl radicals are less prone to recombine. As a result of this, availability of radicals for initiating radical polymerization can be greatly improved. Two commercially available OXEs *O*-benzoyl-*α*-oxooxime (Irgacure OXE-01) and *O*-acetyloxime (Irgacure OXE-02) are well-known to exhibit outstanding curing performances in highly pigmented resist formulations even at low concentrations. These Type I PIs are also useful for the radical polymerization of acrylic monomers.[18, 19] Nevertheless, these OXEs only absorb for rather short wavelengths and their performances decline with increasing wavelength using e.g. near UV LEDs (385 nm, 395 nm) or visible LEDs (405 nm, 415 nm, 450 nm). Hence, recent research studies have been focused on shifting the absorption wavelength of OXEs to the near UV or visible range by introducing different chromophores into their structures (triphenylamine[20], coumarin[21], nitrocarbazole[22], anthracene[23], pyrene[24], phenothiazine[25] etc).

Phenothiazines are nitrogen- and sulfur-containing heterocyclic compounds which have been widely used in the chemical industry because of their pharmacological properties and their applications in solar energy conversion.[26,27] Phenothiazine chromophores have also been employed as photosensitizers along with onium salts in cationic and free radical polymerization reactions[28], but they are only able to initiate polymerization process when excited with broad-band UV irradiation (315–400 nm). Recently, many attempts have been made to shift the absorption of phenothiazine-based photosensitizers into the visible region. Sulfonium salt–phenothiazine initiation systems have notably been used for the cationic photopolymerization of tetrahydrofuran.[29] Thiophene-substituted phenothiazines were used as photosensitizers for *bis*(4-methylphenyl)iodonium hexafluorophosphate (ION) and utilized for both CP and FRP processes[30]. Conjugated phenothiazine oxime esters were also used for the sensitization of ION salt, enabling the FRP of tripropylene glycol diacrylate (TPGDA).[31] Also, phenothiazine derivatives were combined with *bis*-(4-*tert*-butylphenyl)iodonium hexafluorophosphate (Iod) or with (Iod/N-Phenylglycine) for the FRP of TMPTA and the CP of EPOX.[32, 25] All these polymerization reactions were performed under the effect of visible light irradiations. However, the efficiency of these different photoinitiating systems was directly related to the formation of multicomponent photoinitiating systems, complicating the elaboration of photosensitive formulations.

In a previous elegant work, Wang et al. designed three conjugated phenothiazine-based OXEs (Scheme 1) and used them as Type I PIs in the FRP of TPGDA upon exposure to the irradiation of a laser diode at 405 nm and 455 nm.[31] In our work, three new phenothiazine (PTZ) based PIs denoted as (**PTZ1**, **PTZ2** and **PTZ3**) (Scheme 2), have been synthesized and used as monocomponent photoinitiating systems for the FRP of TA. Markedly, parallel to Type I photoinitiating ability, presence of the chromophore also enabled the different phenothiazine derivatives to be used as photosensitizers for the sensitization of an iodonium salt and the resulting two-component photoinitiating systems could be used for the FRP of di(trimethylolpropane)tetraacrylate (TA), the CP of epoxides, and in turn the formation of inter-penetrated polymer networks (IPNs) by the concomitant polymerization of epoxides and acrylates. Photoinitiation ability of the above proposed systems were examined upon exposure to a LED@405 nm. Mechanisms governing the photoinitiation process of the mono and two-component systems were investigated by employing different techniques and characterization methods. Moreover, the thermal initiating behavior was assessed using differential scanning calorimetry (DSC), and their potential use in laser write and 3D printing applications is also presented as a proof of their high reactivity.

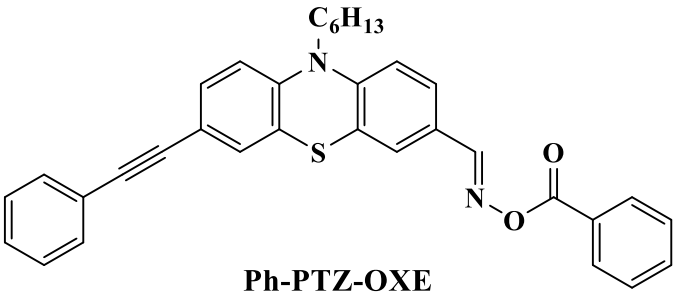

Ph-PTZ-OXE

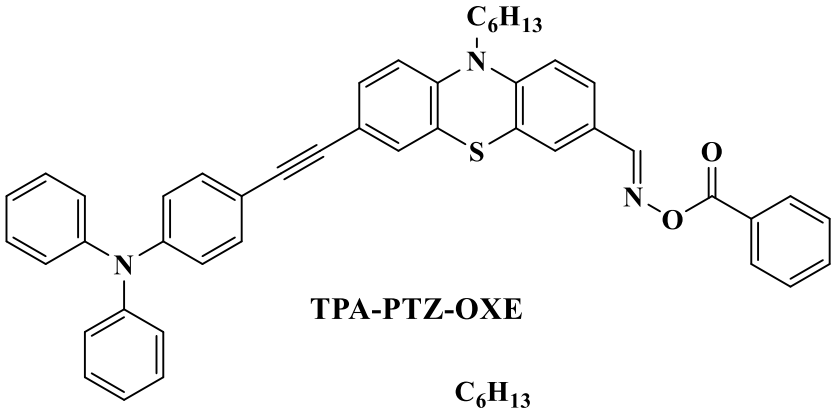

TPA-PTZ-OXE

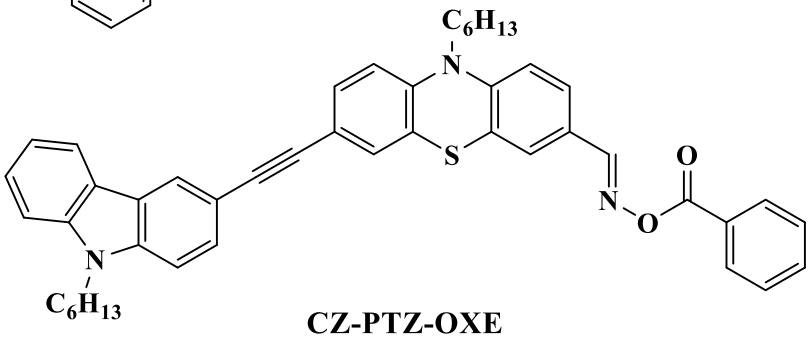

CZ-PTZ-OXE

Scheme 1. Chemical structures and abbreviations of previously investigated conjugated phenothiazine-based OXEs in [31].

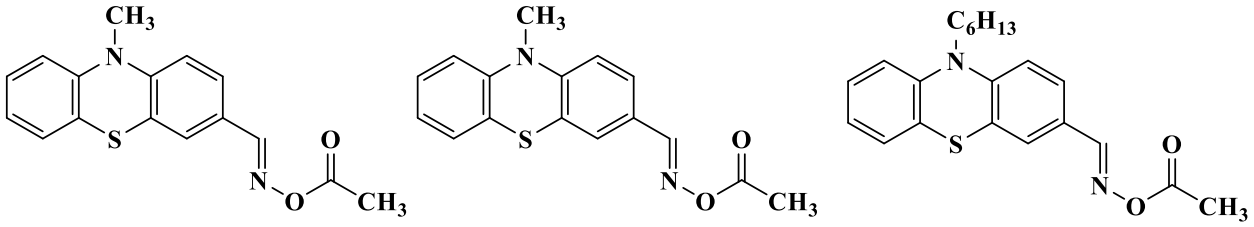

PTZ1 **PTZ2** **PTZ3**

Scheme 2. Chemical structures and abbreviations of the synthesized phenothiazine-based PIs (this work); the hexyl group in PTZ3 has a linear chain structure.

2. Experimental part

2.1. Synthesis of the investigated phenothiazine-based OXEs

The synthesis of the newly proposed photoinitiators (**PTZ1**, **PTZ2** and **PTZ3**) is described in detail in supporting information.

2.2. Other chemical compounds

The chemical compounds used for the preparation of the resin mixtures were selected with the highest purity available and used as received, and their chemical structures are represented in Scheme 3. Diphenyl(2,4,6-trimethylbenzoyl)phosphine oxide (TPO), and *bis*-(4-*tert*-butylphenyl)iodonium hexafluorophosphate (Iod or SpeedCure 938) were obtained from Lambson Ltd (UK). The monomers used i.e. di(trimethylolpropane)tetraacrylate (TA) and (3,4-epoxycyclohexane)methyl-3,4-epoxycyclohexylcarboxylate (EPOX; Uvacure 1500)were obtained from Sartomer-Europe and Allnex, respectively. The storage stabilizer of the acrylate was not removed.

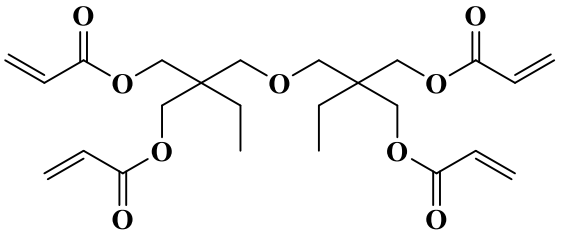

TA

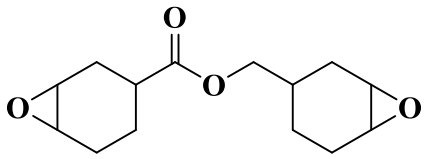

EPOX

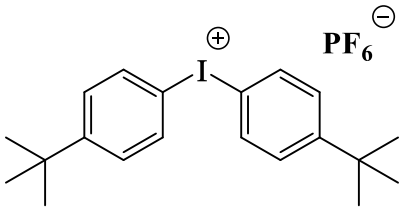

Iod

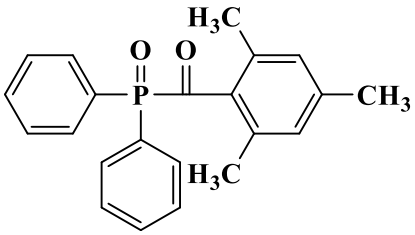

TPO

Scheme 3. Chemical structures and abbreviations of the reference initiator (TPO), the additive (Iod) and the benchmark monomers TA and EPOX.

2.3. Irradiation Sources

Different light-emitting diodes (LEDs) were used as irradiation sources: (1) LED@375 nm with an incident light intensity at the sample surface I_0 = 40 mW·cm^{-2}, and (2) LED@405 nm with an incident light intensity at the sample surface I_0 = 110 mW·cm^{-2}.

2.4. UV-Visible absorption and photolysis experiments

The investigation of the UV-visible absorption properties of PIs in acetonitrile was done by using a JASCO V730 spectrometer. Steady-state photolysis experiments carried out for the different prepared formulations (PIs alone; PIs with Iod (10^{-2} M)) were performed upon exposure to a LED@375 nm, and their associated UV-vis spectra at different irradiation times were measured by means of the JASCO V730 spectrometer. The concentration of PIs used throughout the experiments was 4×10^{-5} M.

2.5. Computational procedure

Molecular orbital calculations were carried out using the Gaussian 03 suite of programs[33, 34]. The electronic absorption spectra for the different compounds were calculated with time-dependent density functional theory at the MPW1PW91/6-31g* level of theory on the relaxed geometries optimized at the UB3LYP/6-31G* level of theory. The triplet state energy levels were also calculated at this level of theory.

2.6. Fluorescence experiment

2.6.1. Steady state fluorescence

The Investigation of the fluorescence properties of PIs in acetonitrile was done by using a JASCO FP-6200 spectrofluorimeter. Fluorescence quenching experiments of PIs by the cumulative addition of Iod (concentrations mentioned in Figure 13) were done by means of the JASCO FP-6200 spectrofluorimeter. The concentration of PIs used throughout the experiments was 4×10^{-5} M.

2.6.2. Time correlated single photon counting (TCSPC)

Fluorescence excited state lifetimes were determined using a time correlated single-photon counting system named HORIBA DeltaFlex with a HORIBA PPD-850 as detector. The excitation source was a HORIBA nanoLED-370 with an excitation wavelength of 367 nm and a pulse duration inferior to 1.4 ns. Fluorescence intensity decay profiles were recorded in DCM in a quartz cell. A

silica colloidal solution LUDOX AS 30, 30 wt % suspension in H_2O was used to evaluate the impulse response function (IRF) of the apparatus.

2.7. Oxidation Potentials

Oxidation potentials for **PTZ** compounds (E_{ox}) were measured by cyclic voltammetry using tetrabutylammonium hexafluorophosphate dissolved in acetonitrile as the electrolyte (potentials vs. Saturated Calomel Electrode – SCE). The free energy change (ΔG_{et}) for an electron transfer reaction was calculated from eqn (1)[35], where E_{ox}, E_{red}, E*, and C stand for the oxidation potential of the electron donor, the reduction potential of the electron acceptor, the considered excited state energy level and the coulombic term for the initially formed ion pair, respectively. Here, the reduction potential of Iod is E_{red}(Iod) = -0.7 V, and C was neglected as usually done for polar solvents.[25]

$$\Delta G_{et} = E_{ox} - E_{red} - E^* + C \qquad (1)$$

2.8. Photopolymerization kinetics (RT-FTIR)

The photopolymerization kinetics of TA and EPOX were obtained by using real-time Fourier transform infrared spectroscopy (JASCO FTIR 6600). For the FRP of TA, the formulations were put in laminate between two propylene films (thickness ~ 25 μm) to reduce O_2 inhibition whereas they were placed on polypropylene films (under air) for the CP of EPOX. Decrease of the C=C double bond peak or the epoxide group band were continuously observed from 1581 to 1662 cm^{-1} or from 768 to 825 cm^{-1} respectively. The final acrylate function conversion of TA and the final epoxy function conversion of EPOX were obtained by using the following equation:

$$\mathrm{FC}\ (\%) = \frac{\mathrm{A0} - \mathrm{At}}{\mathrm{A0}} \times 100$$

Where FC is the final function conversion, A_0 is the proportion of the peak area at 0 sec, and A_t is the portion of the peak area at t s. The prepared formulations (PIs with monomers) were stirred in the dark for 24 h. All the polymerization experiments were performed by using the LED@405 nm at room temperature and the irradiation was initiated after t = 10 s. The weight of the system was calculated from the monomer content. More detailed experimental conditions for each formulation have been noted in the caption of the different figures. The procedure has been already described in Refs. 12 and 36.

2.9. ESR spin-trapping (ESR-ST) experiments

An X-Band spectrometer (Bruker EMX-plus) was used in order to realize the ESR-ST experiments. The experiments were performed out at room temperature (RT) under N_2 with 405 nm LED illumination within the cavity of the ESR spectrometer. Radicals were trapped by XM phenyl-*N*-*tert*-butylnitrone (PBN) obtained from TCI-Europe in *tert*-butylbenzene according to a procedure described in refs. 36 and 37. The PEST WINSIM program was used to obtain the ESR spectrum simulations.

2.10. Differential scanning calorimetry (DSC)

About 10 mg of TA containing 1% wt PI was inserted into a 100 µL aluminum crucible. Thermal polymerization was performed from 25°C to 300°C at a heating rate of 10 °C min^{-1} under nitrogen flow (100 $mL.min^{-1}$). A Mettler Toledo DSC 1 differential scanning calorimeter was used for this purpose.[21]

2.11. Direct laser write and 3D printing experiment

For direct laser writing experiments, a laser diode @405 nm was used for the spatially controlled irradiation. The intensity of laser was 110 mW, and the spot size was 50 µm. The photopolymerization process was done under air and the generated 3D patterns were analyzed using a numerical optical microscope (DSX-HRSU from Olympus Corporation) as presented in the literature[36, 37]. For 3D printing experiments, a SLA 3D Printer (PeoPoly MOAI 130 Printer) was used (λ = 450 nm; Intensity = 150 $mW \cdot cm^{-2}$).

3. Results and discussion

3.1. UV-visible absorption properties

UV-visible absorption spectra of the newly presented PIs recorded in acetonitrile are shown in Figure 1. Their maximum absorption wavelengths (λ_{max}), molar extinction coefficients (ε_{max}) at λ_{max} and at the emission wavelength at 405 nm are assembled in Table 1.

The maximum absorption wavelength (λ_{max}) of the oxime **PTZ1** is located at 325 nm. This value is slightly redshifted upon introduction of the ester functional group in **PTZ2** and **PTZ3** (Figure 1, Table 1). The highest molar extinction coefficient was found for **PTZ3** carrying a hexyl

group as a substituent. This can be confirmed by the HOMO orbital of this molecule (Figure 2), where the first sigma C-C bond of the hexyl group is involved in the enhanced delocalization of electrons. All the investigated PIs revealed high molar extinction coefficients and good absorption properties in line with the emission spectra of the visible LED used in this work.

From the molecular modelling data, the optimized geometries for the different structures and their frontier orbitals (Highest Occupied Molecular Orbital – HOMO and Lowest Unoccupied Molecular Orbital – LUMO) involved in the lowest energy transition are represented in Figure 2. It can be observed that both the HOMO and LUMO are delocalized all over the π-system apparently manifesting a $\pi \rightarrow \pi^*$ lowest energy transition. Moreover, it can be noted that the HOMO's are wrapped on the phenothiazine unit and the LUMO's are also delocalized on the oxime and oxime ester units.

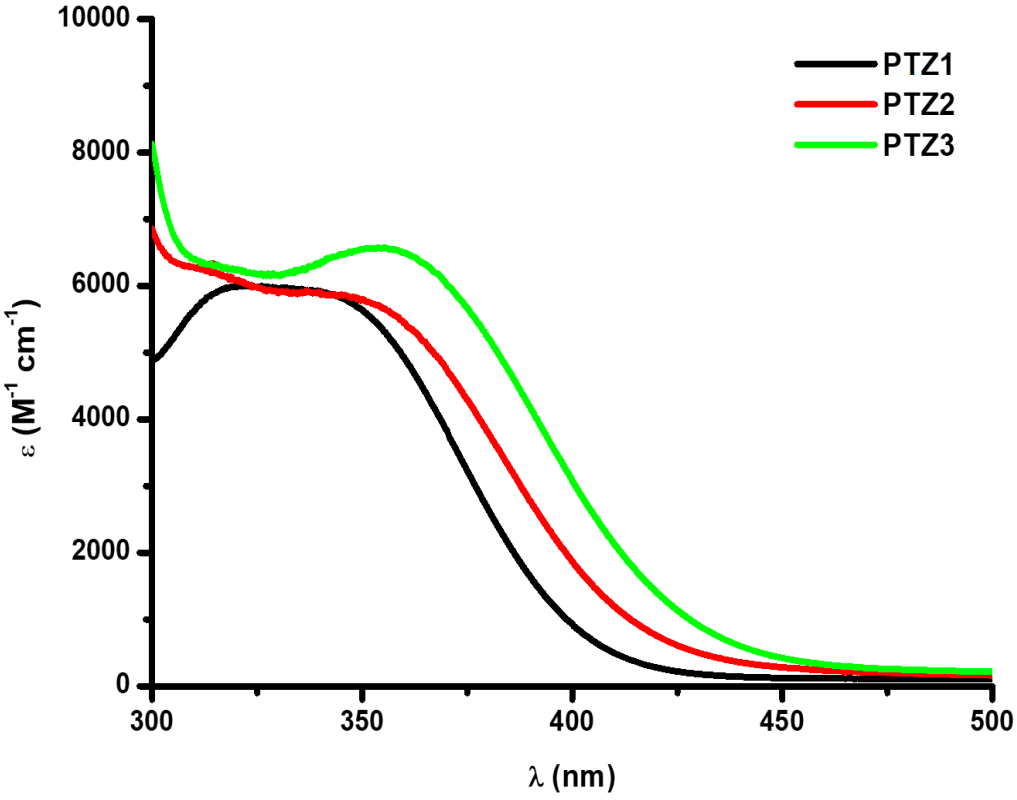

Figure 1. UV-visible absorption properties of compounds **PTZ1-3** in acetonitrile.

Table 1. Light absorption properties of the investigated compounds: maximum absorption wavelength (λ_{max}), and molecular extinction coefficients at λ_{max}, and at 405 nm.

PIs	λ_{max} (nm)	ε_{max} (M^{-1} cm^{-1})	ε_{405} (M^{-1} cm^{-1})
PTZ1	325	6050	665
PTZ2	345	5880	1480
PTZ3	355	6600	2600

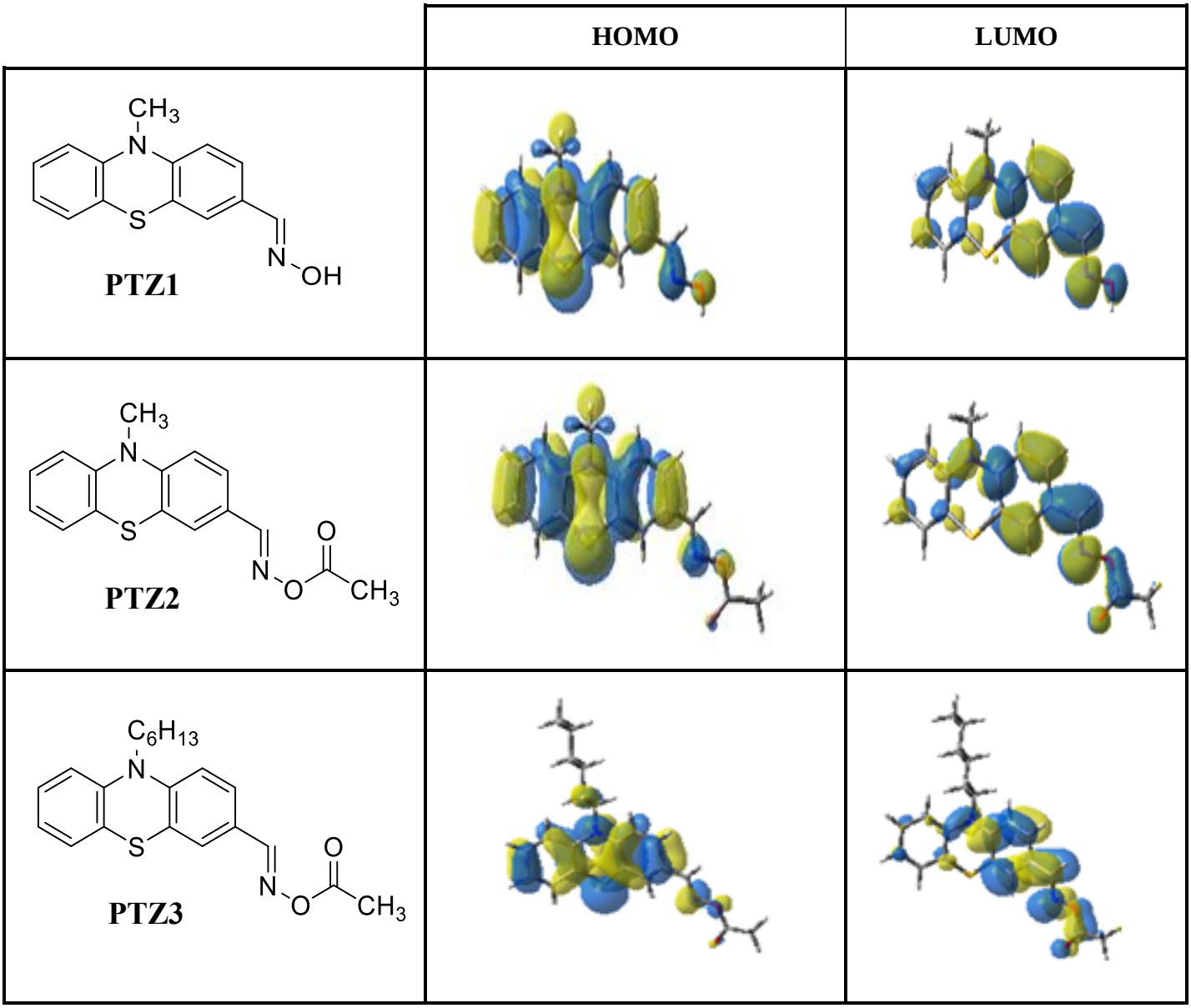

Figure 2. Contour plots of the frontier orbitals (HOMO/LUMO) for PIs; structures optimized at the B3LYP/6-31G* level of theory.

3.2. Type I photoinitiator features

Initiation abilities of the investigated compounds (1% phr) working as mono-component photoinitiating systems for the polymerization of the benchmark TA monomer, were studied using RT-FTIR in thin samples (25 μm, in laminate) under a LED@405 nm. Typical acrylate conversion

versus irradiation time profiles are shown in Figure 3 and the associated final acrylate conversions (FCs) are recapped in Table 2.

PTZ1, the compound which has no oxime-ester functional group, showed a long inhibition period followed by a small polymerization rate in the FRP of TA.

PTZ2 and **PTZ3** i.e. two compounds with a methyl substituent on the carboxyl side showed fast polymerization rates as well as high final conversions, which is not only related to their good absorption properties but also to other factors including the cleavage process, the decarboxylation reaction, and the reactivity of the generated radicals[21]. This accentuate the significant role of the oxime-ester function to act as a Type I PI. **PTZ3** (with a hexyl substituent attached to the phenothiazine chromophore) reached the highest FC (81%) which renders it as an efficient PI by comparing it with the commercial benchmark PI (TPO; FC = 83%) (See Fig. 3 and Table 2), in agreement with the good absorption properties and high molar extinction coefficient related to **PTZ3**.

Other phenothiazine-based OXEs bearing a hexyl chain for solubility denoted as (**Hex1→Hex10**) (Scheme S1) or bromine substituent to modify the absorption maxima denoted as (**1A→13A**) (Scheme S2) achieved also high final conversions of the acrylate functional group of the TA monomer (See Figures S1 and S2). In this series of photocleavable groups, it can be noticed that all OXEs with an acetyl group on the oxime ester moiety (like **PTZ2** and **PTZ3**) exhibited the best photoinitiation ability compared to the other OXEs having different substituents (**Hex1→Hex10** and **1A→13A**). This higher photoinitiating ability can be assigned to the favorable enthalpy of decarboxylation reaction in the case of the methyl substituent (CH_3-C(=O)O$^\bullet$ → $CH_3^\bullet$ + CO_2; $\Delta H_{decarboxylation}$ = - 4.94 Kcal mol^{-1})[21].

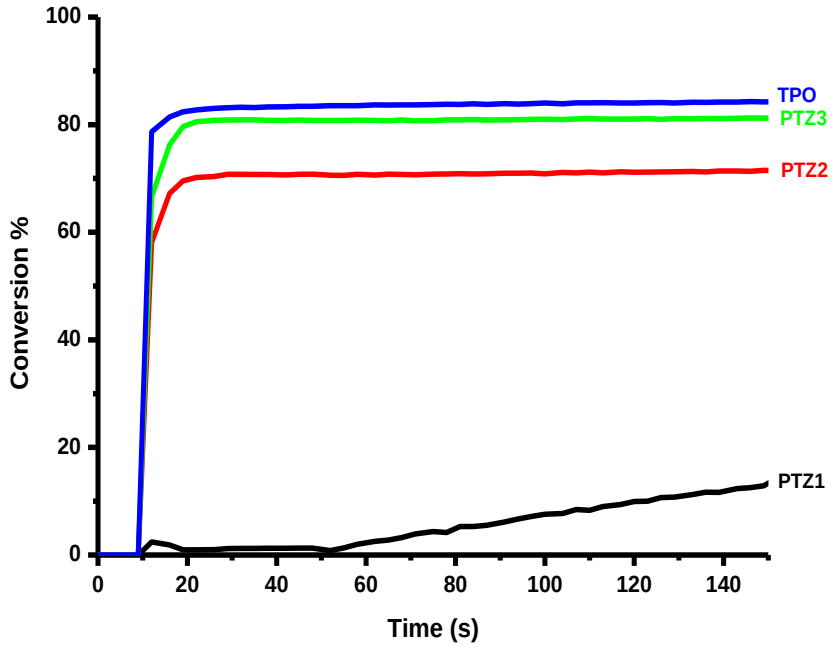

Figure 3. Photopolymerization profiles of TA (acrylate function conversion vs. irradiation time) in laminate (thickness = 25 µm) upon exposure to a LED (λ = 405 nm) in the presence of PIs (1%w/w). The irradiation starts at t = 10 s.

Table 2. FCs of acrylate function using one component photoinitiating system (1% w/w) after 150 s of irradiation with a LED (λ = 405 nm).

PIs	Thin samples (25 µm) in laminate @405 nm
TPO	83%
PTZ1	14%
PTZ2	71%
PTZ3	81%

The detection of CO_2 release consequent to the polymerization of TA monomer confirms the occurrence of a decarboxylation reaction in the photoinitiation mechanism. The infrared spectra obtained by real time Fourier transformed infrared spectroscopy (RT-FTIR) before and after polymerization and presented in Figures 4 (A) and (C) show a peak appearance at 2337 cm^{-1} for both **PTZ2** and **PTZ3** which proves the release of CO_2. The positive correlation between CO_2 release and the efficiency of the polymerization process for both **PTZ2** and **PTZ3** illustrated in Figures 4 (B) and (D) emphasize the prominent role of the decarboxylation step in yielding

initiating radicals for the polymerization process. These results are in agreement with the favorable enthalpy of decarboxylation reaction observed in the case of methyl substituent.

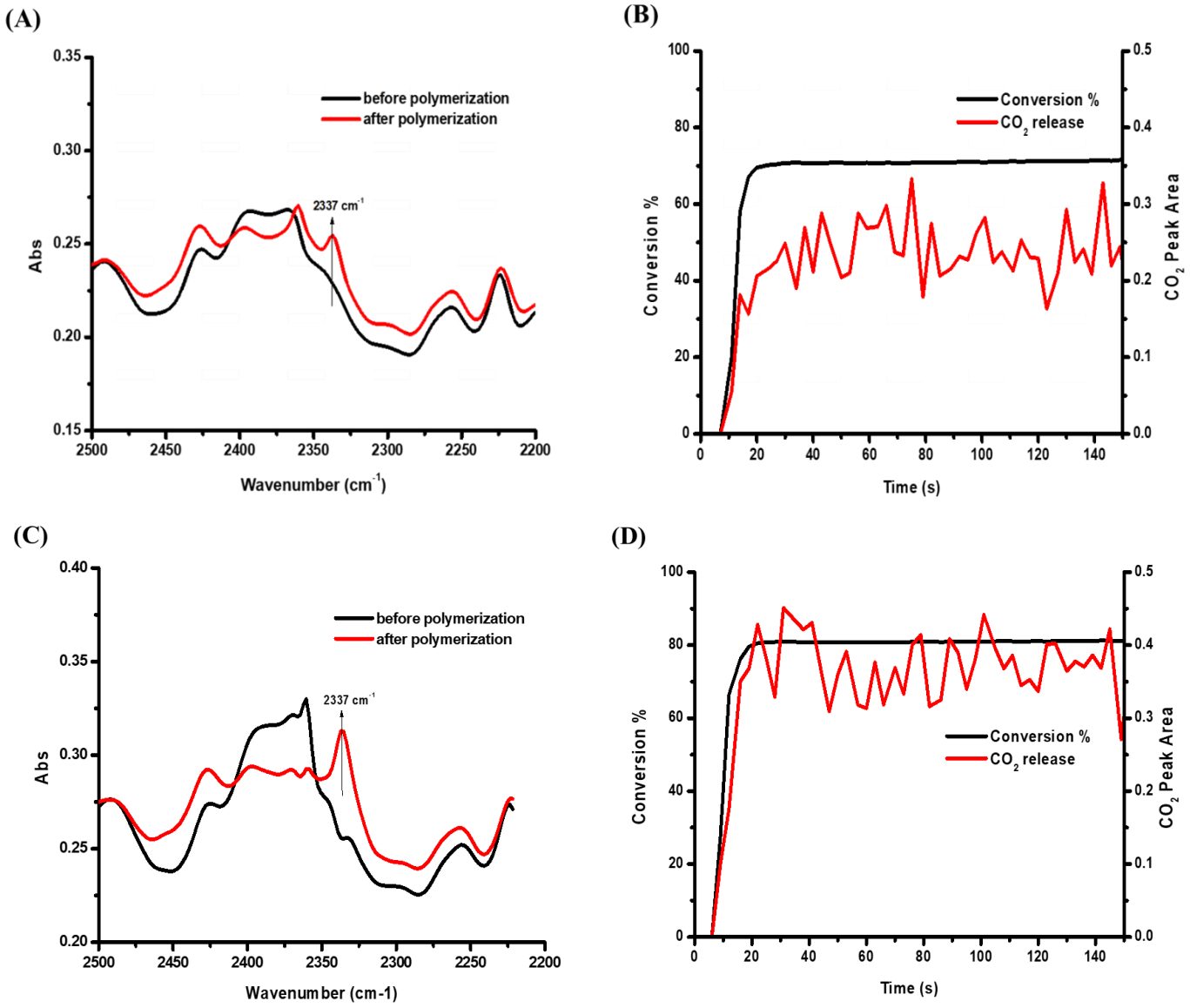

Figure 4. (A) and (C) Detection of CO_2 released during photopolymerization using **PTZ2** and **PTZ3** respectively; (B), and (D) conversion-decarboxylation correlation using **PTZ2** and **PTZ3** respectively; PI (1% w/w) in TA (thin film polymerization @ 405 nm in laminate).

With aim at confirming the occurrence of a cleavage process and the detection of the type of initiating radicals in the decarboxylation step, ESR spin trapping experiments have been performed. Two kinds of radicals were trapped by PBN for the **PTZ3** photolysis after 60 s of irradiation (See

Figure 5). Values of the hyperfine coupling constants for the first radical adduct (75.5%) were α_N = 13.5 G and α_H = 1.8 G which could be assigned to the acetoxy radical ($CH_3COO^{\bullet}$). Thus, the cleavage of the N-O bond in **PTZ3** under irradiation and the formation of acetoxy radicals were confirmed. Another free radical adduct (24.5%) with hyperfine coupling constants α_N = 14.5 G and α_H = 3.8 G which could be assigned to the methyl radical ($^{\bullet}CH_3$). Therefore, we can say that a portion of the acetoxy radicals are decomposed into CO_2 and methyl radicals during the decarboxylation step. The results obtained are in agreement with the CO_2 release detected by FT-IR in the photopolymerization process (Figure 4). Based on the above results, a photoinitiation mechanism of phenothiazine based OXEs could be confirmed in this study and the details are shown in Scheme 4. This mechanism is quite similar to the photo-Kolbe reaction which was done and proven before.[38, 39]

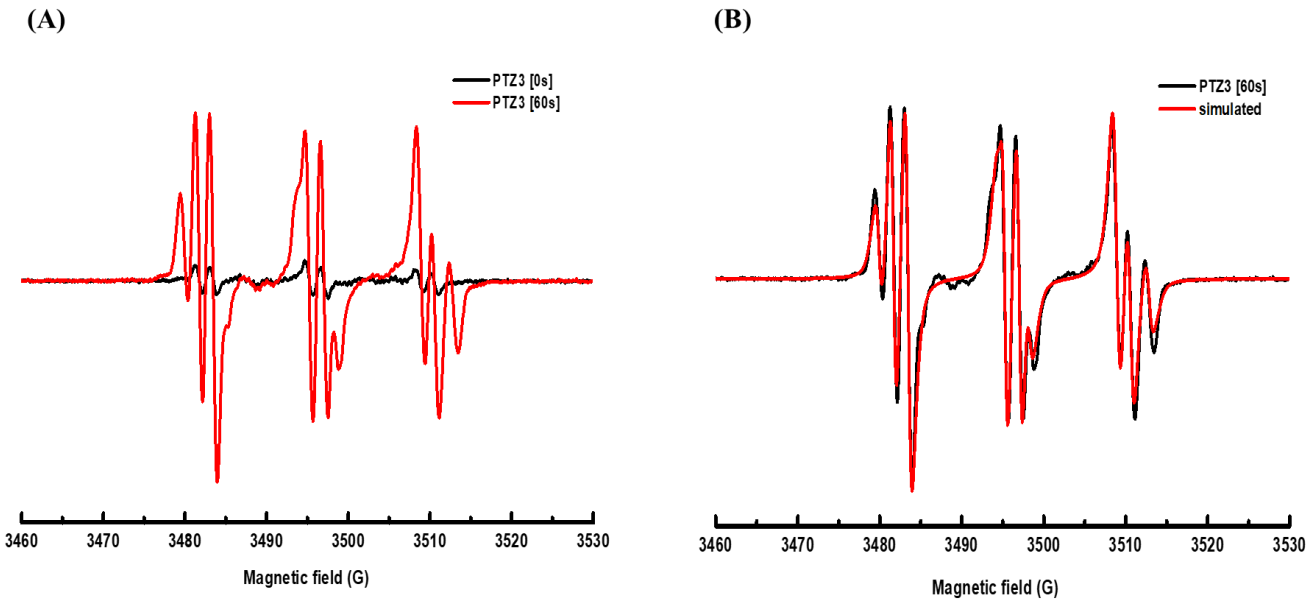

Figure 5. ESR spectra for **PTZ3** recorded in the presence of PBN and *tert*-butylbenzene with a LED@405nm: (A) before and after irradiation; (B) experimental and simulated spectra observed after irradiation (at t = 60 s).

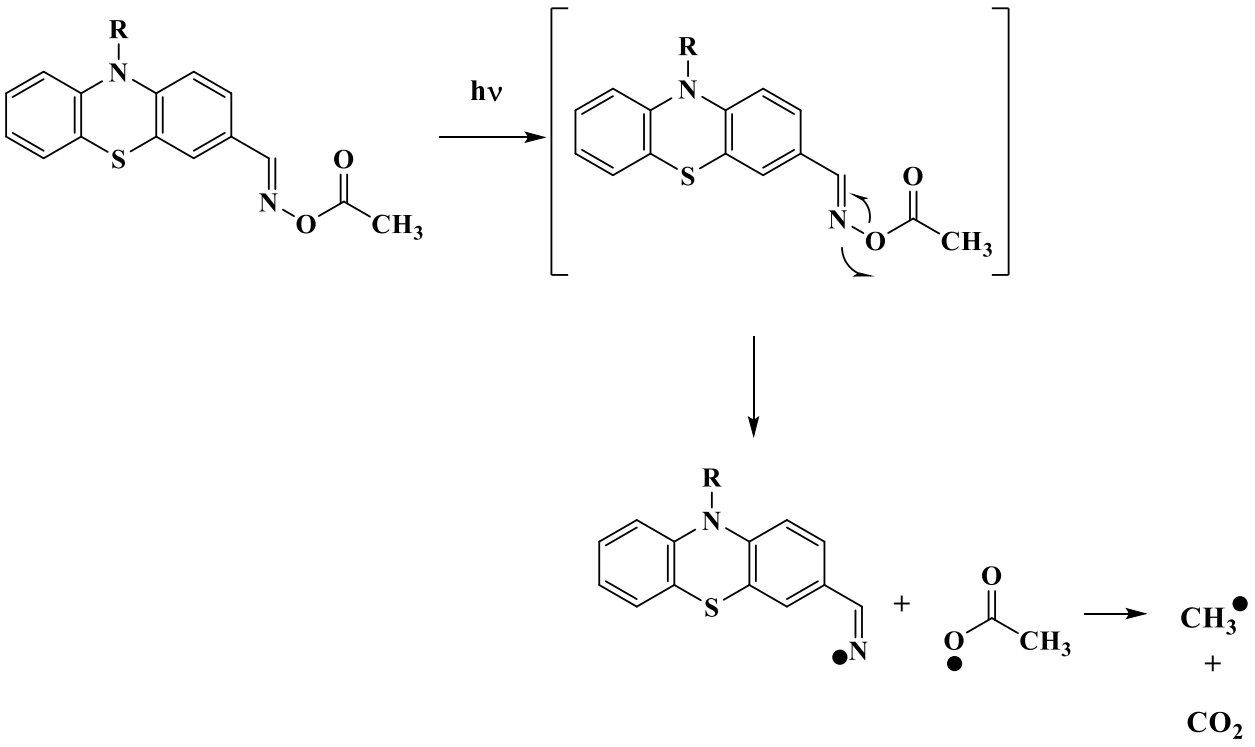

Scheme 4. Proposed photochemical mechanism for phenothiazine-based oxime esters.

In order to study the photochemical properties of PIs, steady-state photolysis was performed in acetonitrile upon exposure to a LED@375 nm. The results presented in Figure 6 (A), (B), and (C) for **PTZ1**, **PTZ2**, and **PTZ3** respectively have shown a modest decline of the absorbance intensity at the maximum wavelength in **PTZ1** (without an oxime-ester functionality) compared to **PTZ2** and **PTZ3** where we could notice a rapid decrease of the absorbance intensity after 10 to 60 s of irradiation, which evidently highlights the impact of the oxime-ester functionality in the photoreaction occurrence. These photolysis results are in agreement with the poor Type I behavior of **PTZ1** and the affluent Type I behavior of **PTZ2** and **PTZ3** observed during the photopolymerization experiments.

The energy needed for the dissociation of the N-O bond (BDE), the singlet excited state energy E_{S1} (determined from the crossing point of the absorption and fluorescence spectra (Figure 6 (D)), and the triplet excited state energy E_{T1} for the studied compounds are gathered in Table 3. We can notice that the $BDE_{N\text{-}O\ bond}$ for all compounds is higher than their triplet excited state energies E_{T1}, and thus the cleavage processes from T_1 are not energetically favorable ($\Delta H_{cleavageT1} = BDE - E_{T1} > 0$) whereas it is lower than their singlet excited state energies E_{S1}, suggesting a

cleavage occurring from S_1 ($\Delta H_{cleavageS1}$ = BDE - E_{S1} < 0). The fluorescence lifetime of the phenothiazine-based oxime esters was also measured and the values are gathered in Table 3 and Figure 6 (E). **PTZ1** showed the longest lifetime (7.65 ns), which decreased upon introduction of the oxime-ester function up to 7.1 ns in **PTZ2** and 7.06 ns in **PTZ3**, demonstrating a cleavage occurring from the S_1 state in agreement with the negative favorable enthalpy for the singlet excited state obtained above.

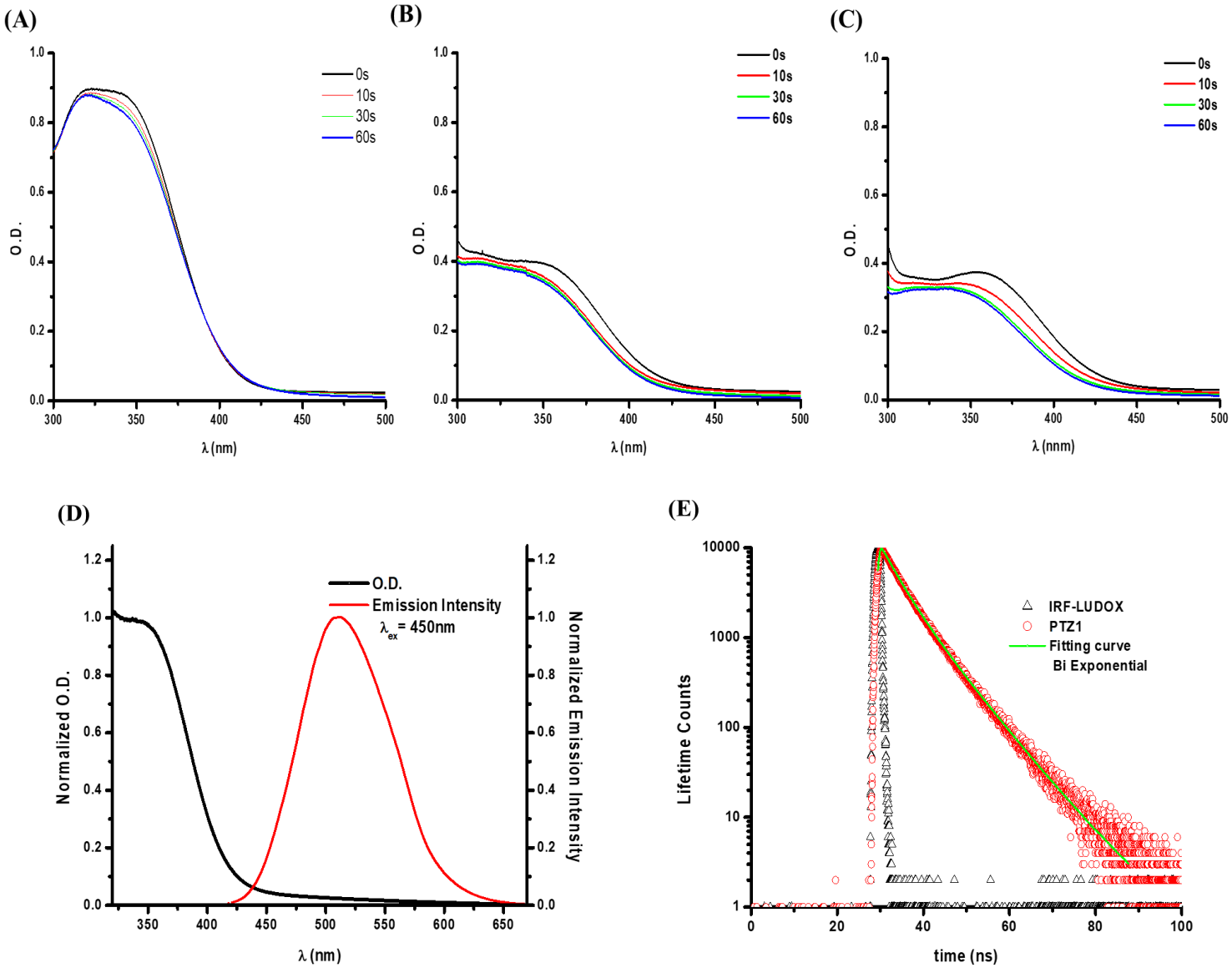

Figure 6. Photolysis of (A) **PTZ1**, (B) **PTZ2**, and (C) **PTZ3** in acetonitrile using LED at λ = 375 nm. (D) UV-visible absorption and emission spectra of **PTZ2** in acetonitrile. (E) Time correlated single-photon counting of **PTZ1** in acetonitrile, λex = 367 nm, λem = 491 nm.

Table 3. Parameters characterizing **PTZ1-PTZ3**. Parameters calculated by molecular modelling: the bond dissociation energy BDE (N–O), the triplet state energy E_{T1}. The enthalpy ($\Delta H_{cleavageT1}$) for the cleavage process from T_1 ($\Delta H_{cleavageT1}$ = BDE – E_{T1}), the singlet excited state energy E_{S1} (evaluated from the experimental absorption and fluorescence spectra), the enthalpy ($\Delta H_{cleavageS1}$) for the cleavage process from

PI	N-O BDE (kcal/mol)	E_{S1} (kcal/mol)	τ_0 (S_1) (ns)	$\Delta H_{cleavageS1}$ (kcal/mol)	E_{T1} (kcal/mol)	$\Delta H_{cleavageT1}$ (kcal/mol)
PTZ1	65.12	65.72	7.65	-0.6	53.62	11.5
PTZ2	54.34	65.128	7.1	-10.78	48.67	5.67
PTZ3	54.28	64.25	7.06	-9.97	48.65	5.63

S_1 ($\Delta H_{cleavageS1}$ = BDE - E_{S1}).

3.3. Use in 3D printing

Because of its considerable photoinitiation ability during the free radical polymerization process of TA, **PTZ3** (0.1% w/w) was selected as an appropriate system to perform the direct laser write (DLW) and 3D printing experiments. The denotation "PTZ" shown in Figure 7(A) was obtained through DLW by using a laser diode @405 nm and characterized by numerical optical microscopy. Appealingly, the obtained 3D pattern has a great thickness (≈ 1570 µm), high spatial resolution, and it requires a very short irradiation time to be generated (15 s) which confirms the high photosensitivity of **PTZ3**. Additionally, and according to a computer model, a 3D cube (thickness ≈ 4.2 mm; thickness of each layer = 20 µm) was fabricated successfully by using a PeoPoly MOAI 130 Printer (Figure 7(B)).

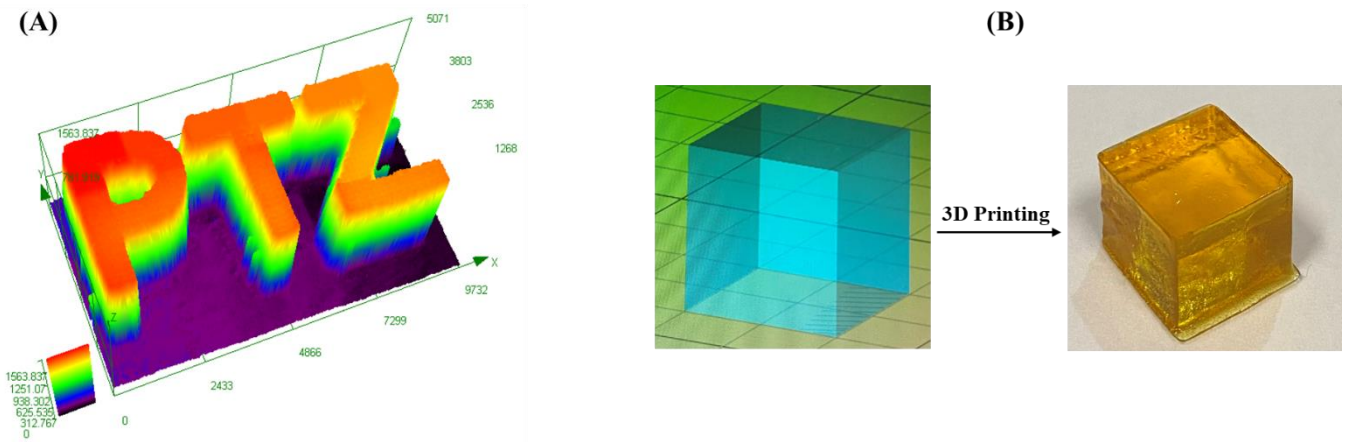

Figure 7. (A) 3D pattern obtained upon exposure to a laser diode @405 nm characterized by numerical microscopy for compound **PTZ3** (0.1% w/w) in TA. (B) 3D printing experiments using a 3D printer for compound **PTZ3** (0.5% w/w) in TA (thickness = 4.2 mm).

3.4. Thermal initiator features

In the purpose of studying the thermal initiator features of our phenothiazine-based PIs after manifesting their photoinitiating abilities during the FRP of TA under LED @ 405 nm, two-cycle DSC experiments of **PTZ1**, **PTZ2**, and **PTZ3** in TA have been performed and their associated curves (temperature vs heat flow) are presented in Figure 8. The onset temperature of thermal polymerziation (T_{Onset}), the temperature of maximum polymerization rate (T_{max}), and the final acrylate FCs of TA are given in Table 4. Markedly, the importance of the oxime-ester functionality for thermal polymerization initiator behavior is noticed with a decline in T_{max} from 241 °C in **PTZ1** (without OXE function) to nearly 170 °C in **PTZ2** and **PTZ3**. Moreover, it can be seen that oxime **PTZ1** needs a temperature of 206 °C to start the polymerization, which decreases significantly after the introduction of the oxime ester moiety in **PTZ2** and **PTZ3**.

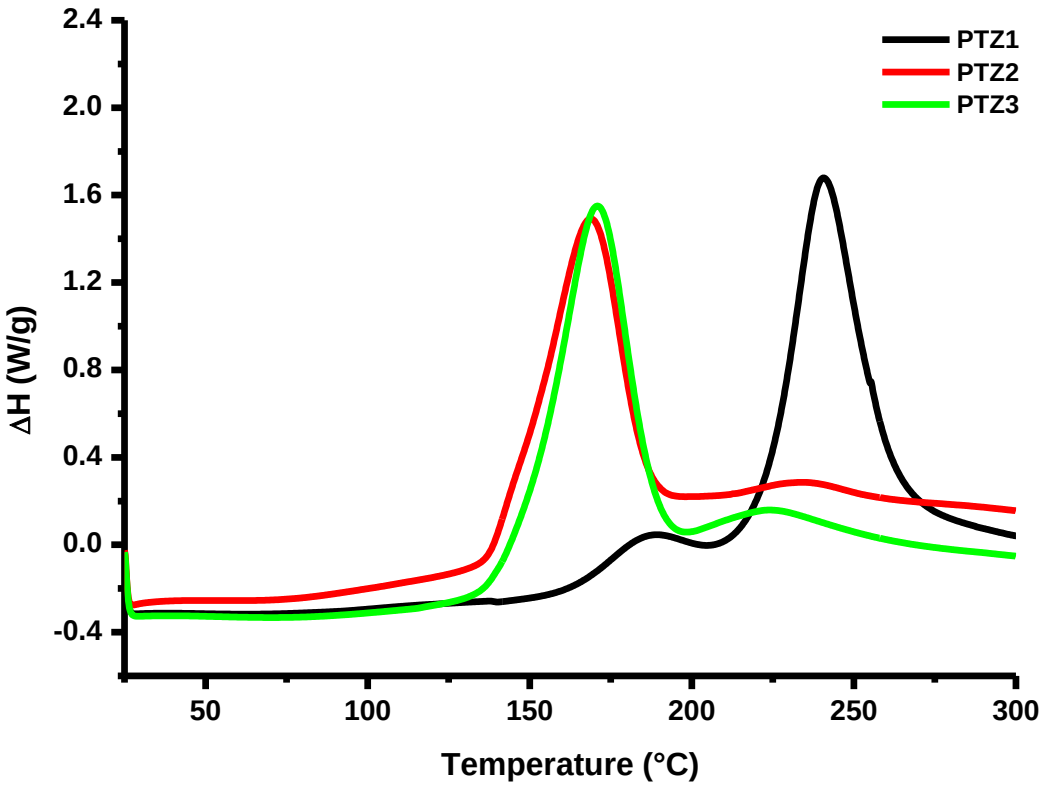

Figure 8. Thermal polymerization experiments (Enthalpy versus heating temperature) of one component initiating systems (1% w) in TA.

Table 4. Maximal, onset polymerization temperatures and final acrylate FCs for TA using **PTZ1**, **PTZ2**, and **PTZ3** (1%w) as thermal initiators under N_2.

PIs	T_{Onset} (°C)	T_{max}(°C)	[a] Conversion (%)
PTZ1	206	241	37
PTZ2	135	169	34
PTZ3	125	171	36

[a] : The heat released for the acrylate double bond is ΔH_{theory} = 78.61 kJ mol^{-1} which leads to 674.8 J g^{-1} for 100% of acrylate function conversion for TA, so the final acrylate function conversion (FC) = (heat released per g)/674.8 is obtained in thermal polymerization.

3.5 Multi-component photoinitiating system features

The photoinitiation abilities of the different derivatives in the presence of an iodonium salt as an additive (1% w/w) for the FRP of TA acrylate monomer were also tested upon irradiation with a LED@405 nm. Typical acrylate function conversion vs. irradiation time profiles are presented in Figure 9 and the associated final acrylate function conversions (FCs) are summed up in Table 5.

The experimental results show that the addition of an iodonium salt has a favorable impact on the final acrylate function conversion compared to those obtained with PTZ derivative alone. This impact is clearly observed for **PTZ1** and **PTZ2** where the FC increases from 14% to 68% for **PTZ1** and from 71% to 82% for **PTZ2** (See Figure 9 and Figure 3). It should be noted that the iodonium salt alone was unable to initiate the FRP of TA under the same conditions, clearly showing the importance of the PTZ derivative for an efficient process. The efficiency trend for the PTZ/Iod couples determined during the FRP of TA respects the following order: **PTZ3**≈**PTZ2**>**PTZ1** which is not only related to the absorption properties of the investigated PIs, but also to their photochemical reactivity with the iodonium salt and the yield of electron transfer to generate the initiating aryl radicals $Ar^{\bullet}$ (Equations (r1) and (r2) below).

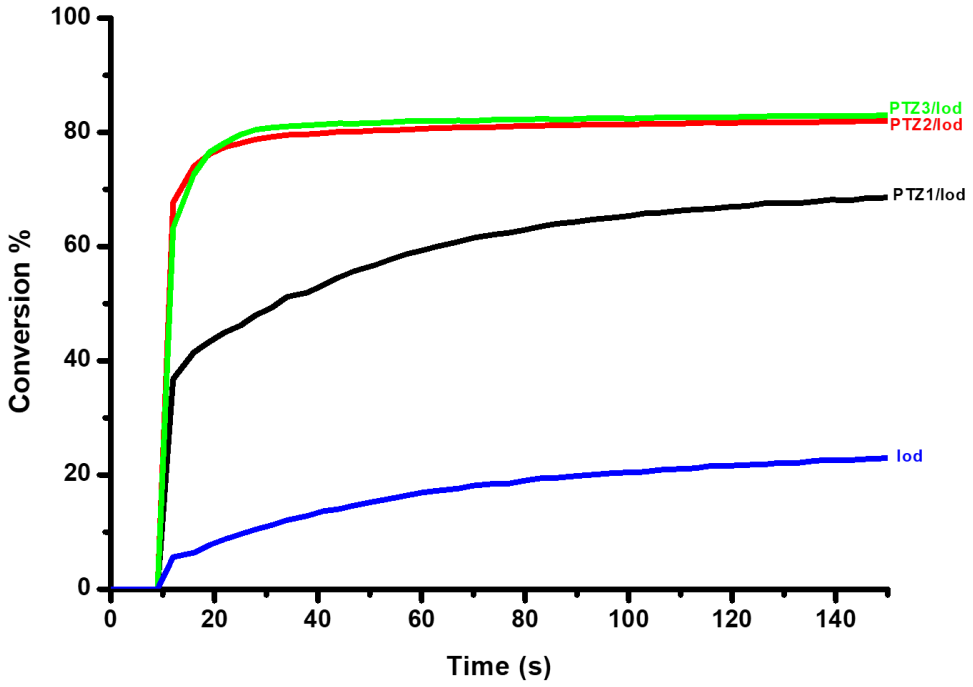

Figure 9. Photopolymerization profiles of TA (acrylate function conversion vs. irradiation time) in laminate (thickness = 25 µm) upon exposure to a LED (λ = 405 nm) in the presence of PI/Iod (1%/1% w/w) and Iod alone (1% w/w). The irradiation starts at t = 10 s.

Table 5. FCs of acrylate function using two component photoinitiating system PI/Iod (1%/1% w/w) and Iod alone (1% w/w) after 150 s of irradiation with a LED (λ=405 nm).

	Thin samples (25 µm) in laminate @405 nm
PTZ1/Iod	68%
PTZ2/Iod	82%
PTZ3/Iod	83%
Iod	23%

The CP of EPOX upon LED irradiation @405 nm was also investigated by using our PIs as photosensitizers for iodonium salt (Iod). Epoxy function conversion versus irradiation time profiles are shown in Figure 10 and the associated final epoxy conversions (FCs) are gathered in Table 6.

The obtained results showed that the CP of EPOX in the presence of a bi-component system (PI/Iod) is very efficient in terms of polymerization rate (Rp) and final epoxy function conversion (FCs) where it reaches 83% for the **PTZ2**/Iod system. Iod alone in EPOX showed a poor

polymerization behavior in agreement with its lack of absorption at 405 nm which highlights the importance of PTZ derivatives for designing an efficient photoinitiating system. The efficiency trend for the PI/Iod couples determined during the CP of EPOX respects the following order: **PTZ2>PTZ1>PTZ3** which is not only linked to the absorption properties of the investigated PIs, but also to their photochemical reactivities with the iodonium salt and the yield of electron transfer to generate the initiating radical cations $PTZ^{\bullet+}$ (Equations (r1) and (r2) below).

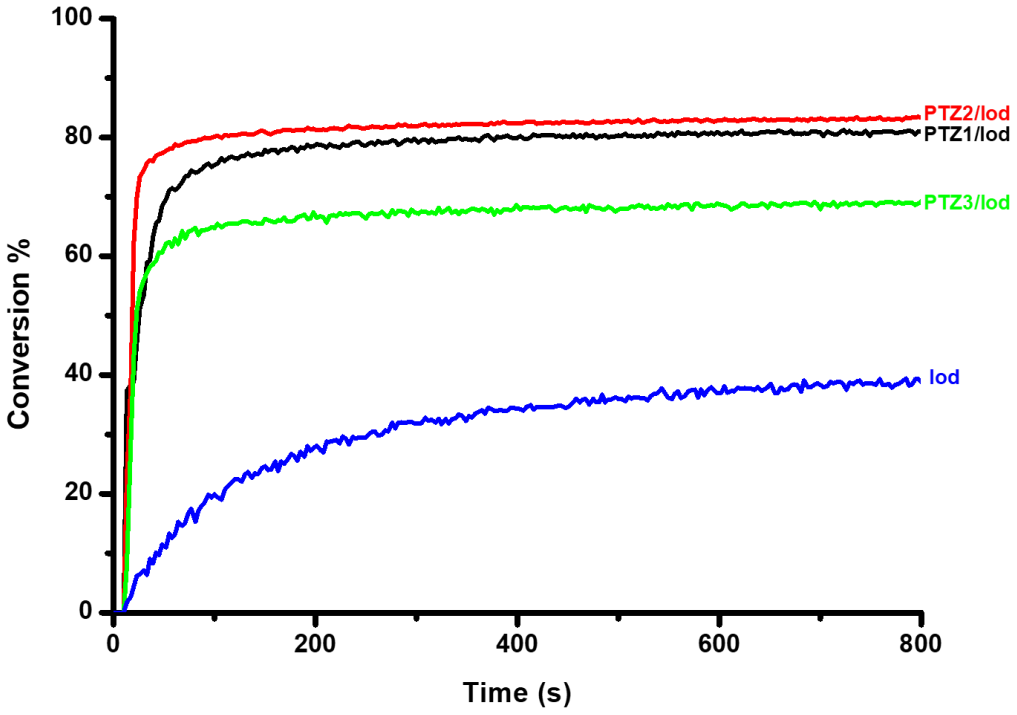

Figure 10. *Photopolymerization profiles of EPOX (epoxy function conversion vs. irradiation time) under air (thickness = 25 µm) upon exposure to a LED (λ = 405 nm) in the presence of PI/Iod (1%/1% w/w) and Iod alone (1% w/w). The irradiation starts at t = 10 s.*

Table 6. FCs of epoxy function using two component photoinitiating system PI/Iod (1%/1% w/w) and Iod alone (1% w/w) after 800 s of irradiation with a LED (λ = 405 nm).

	Thin samples (25 µm) in laminate @405 nm
PTZ1/Iod	81%
PTZ2/Iod	83%
PTZ3/Iod	69%
Iod	38%

The synthesis of Interpenetrated Polymer Networks (IPN) by combining both free radical and cationic polymerization processes is interesting because it combines the advantages of both processes without their respective disadvantages. Acrylate and Epoxy function conversion versus irradiation time profiles for **PTZ2**/Iod system and Iod alone are shown in Figure 11, and those for **PTZ1**/Iod and **PTZ3**/Iod systems are shown in supporting information (Figure S3 and Figure S4 respectively). The associated final acrylate and epoxy conversions (FCs) for all systems are summarized in Table 7.

The final acrylate and epoxy functional groups conversions (FCs) showed that the different PI/Iod systems can initiate the hybrid polymerization of TA/EPOX blend (50%/50% wt/wt). **PTZ2** and **PTZ3** achieved the highest TA monomer conversions with an acrylate function reaching a FC = 99%, whereas **PTZ1** achieved the higher polymerization of the EPOX function reaching a FC = 91%. Iod alone without the presence of dyes showed its inability to form IPNs.

Reactivity of PTZs is clearly influenced by different effects. First, for **PTZ2** and **PTZ3** that are very reactive in FRP, it can be assumed that the solidification due to the FRP is very fast preventing an efficient cationic polymerization (epoxy conversion < 53% ; Table 7) as vitrified state is rapidely reached. For **PTZ1** system, the FRP is not very efficient (see Figure 3 above) and therefore the CP pathway can be more favourable (epoxy conversion =80% ; Table 7). Due to the same effect, the final double bond conversions of the PTZ2 and PTZ3 systems are so exceptionally high. The initiator and monomer dissolved in the liquid EPOX phase have significant mobility, so that the acrylic esters are almost completely consumed.

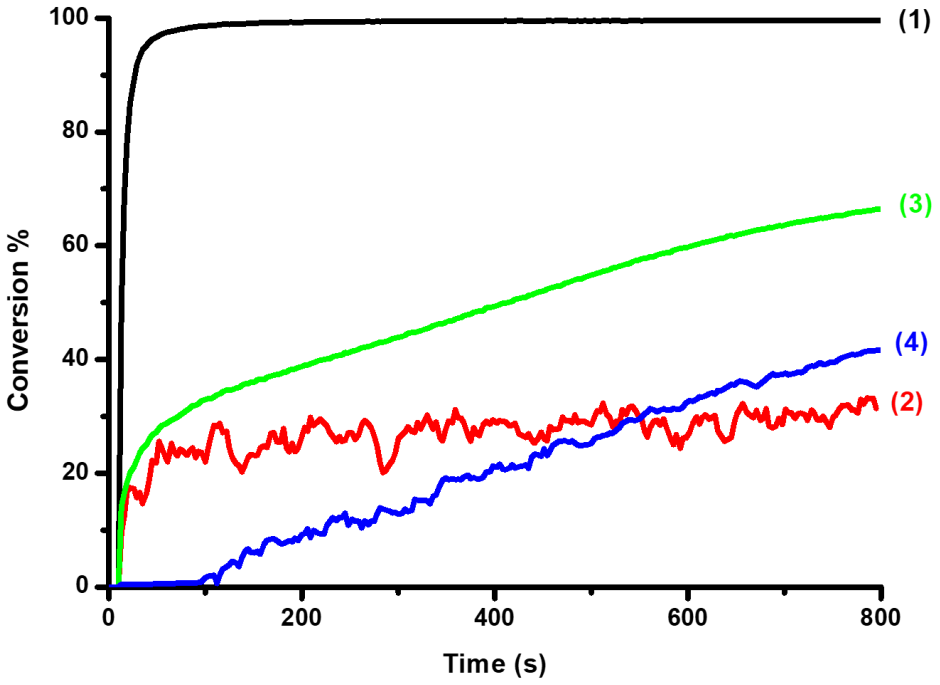

Figure 11. Polymerization profiles for TA/EPOX blend (50%/50%) in laminate (thickness = 25 μm) upon exposure to a LED (λ = 405 nm) in the presence of **PTZ2**/Iod (1%/1% w/w): (1) acrylate functions; (2) epoxy functions, and in the presence of Iod alone (1% w/w): (3) acrylate functions; (4) epoxy functions.

Table 7. Final acrylate or epoxy function conversions (FCs) for the polymerization of TA/EPOX blend (50%/50% w/w) using two component photoinitiating system PI/Iod (1%/1% phr) after 800 s of irradiation with LED light (λ = 405 nm).

	Thin samples (25 μm) in laminate @405 nm	
	Acrylate function	**Epoxy function**
PTZ1/Iod	72%	80%
PTZ2/Iod	99%	33%
PTZ3/Iod	99%	53%

Steady-state photolysis experiments of the PI/Iod (10^{-2} M) systems were performed in acetonitrile under light irradiation (LED@375 nm). We can observe a fast photolysis occurring in the presence of Iod which evidently reveals the favorable interaction between the investigated PIs in their excited singlet states with the iodonium salt besides the N-O bond cleavage process, in

agreement with the results obtained in the photopolymerization experiments. Isobestic points were also observed suggesting photochemical processes without side reactions.

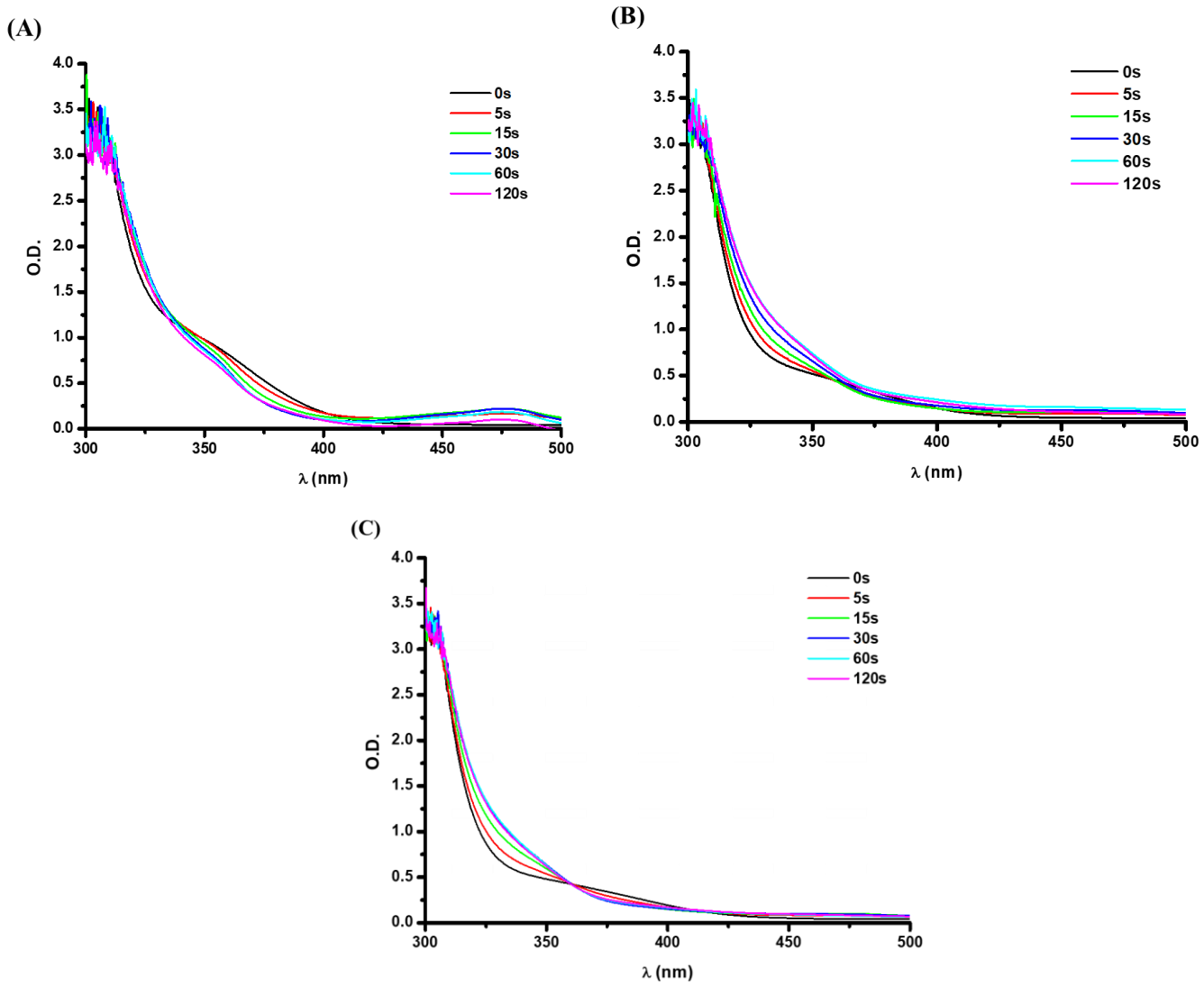

Figure 12. Photolysis of (A) **PTZ1**, (B) **PTZ2**, and (C) **PTZ3** with Iod (10^{-2} M) in acetonitrile using LED at λ = 375 nm.

In order to better understand the interaction between the new PIs and the iodonium salt (Iod), fluorescence quenching experiments were carried out in acetonitrile. The concentration of Iod was increased consecutively and each time a fluorescence spectrum was obtained. Figure 13 shows a

rapid fluorescence quenching occurring for **PTZ1**, **PTZ2**, and **PTZ3** by Iod, which evidently verifies the strong interaction of our PIs with Iod (as shown in Equations (r1) and (r2)).

The oxidation potentials (E_{ox}) determined by cyclic voltammetry allowed the evaluation of the free energy change (ΔG) for this electron transfer reaction (Table 8). Highly favorable ΔG are found in accordance with the strong PI/Iod interaction observed in the fluorescence quenching experiments. High electron transfer quantum yields (Φ_{et}) (92%, 89%, 87% for **PTZ1**, **PTZ2**, and **PTZ3** with Iod respectively) were obtained according to the following equation: $\Phi_{et} = k_{sv}[Iod]/(1 + k_{sv}[Iod])$.

$$PTZ\ (h\upsilon) \rightarrow {}^{1}PTZ \qquad (r1)$$

$${}^{1}PTZ + Ar_2I^{+} \rightarrow PTZ^{\bullet+} + Ar^{\bullet} + ArI \qquad (r2)$$

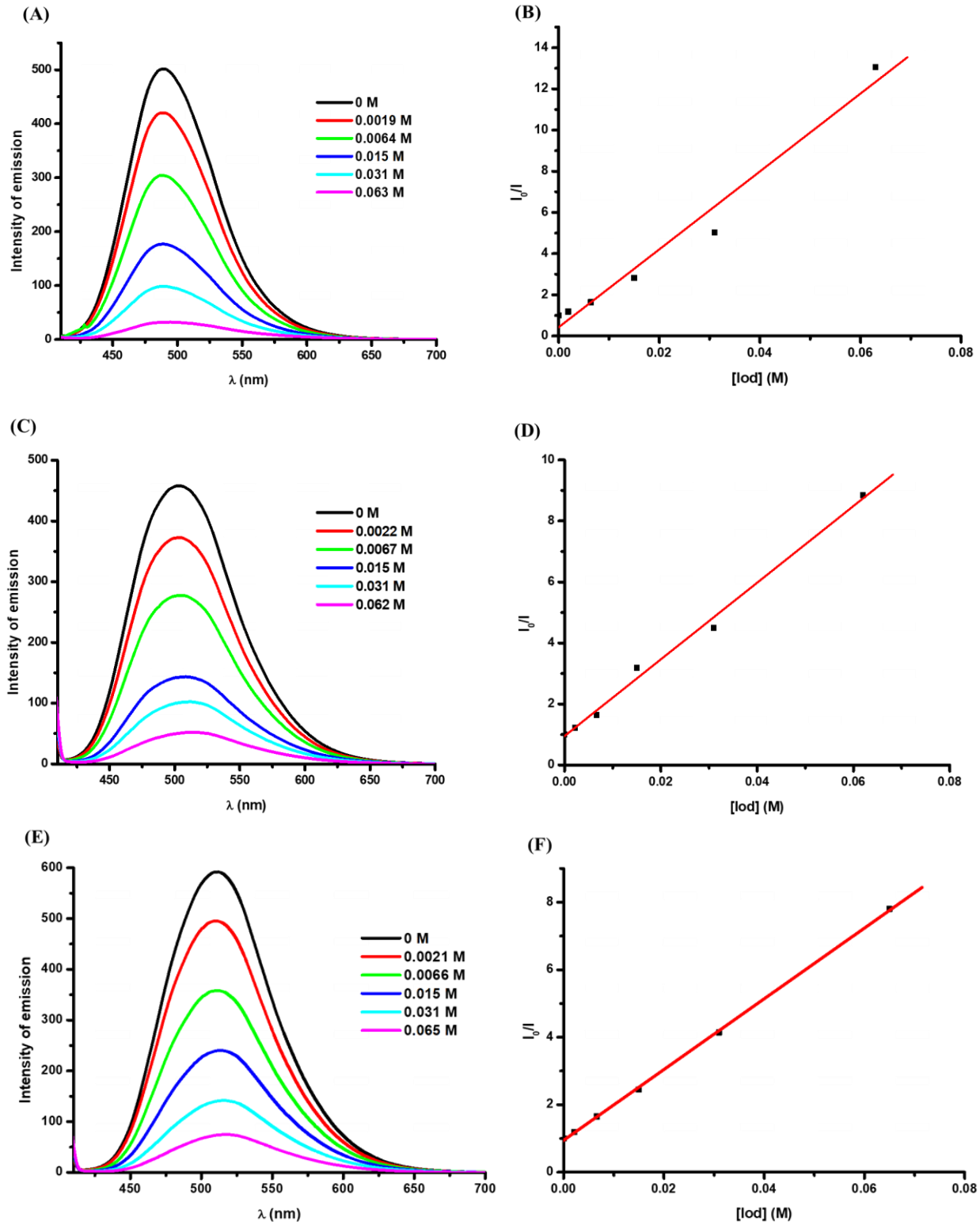

Figure 13. Fluorescence quenching study of **PTZ1** (A), **PTZ2** (C), and **PTZ3** (E) by Iod in acetonitrile. Associated Stern-Volmer plot of **PTZ1** (B), **PTZ2** (D), and **PTZ3** (F).

Table 8. Parameters characterizing the chemical mechanisms associated with the PI/Iod interaction in acetonitrile.

PI	E_{ox} (eV)	E_{S1} (eV)	$\Delta G_{S1\ (Iod)}$ (eV)	K_{sv} (M^{-1})[a]	$\Phi_{et\ (OXE/Iod)}$
PTZ1	0.73	2.89	-1.46	189	0.92
PTZ2	0.79	2.82	-1.33	126	0.89
PTZ3	0.74	2.78	-1.34	105	0.87

[a] *: Stern-Volmer coefficient (Ksv): slope of the quenching curve ($I_0/I = 1+Ksv[Iod]$).*

In the aim of confirming the quenching process of **PTZ1** by Iod and the detection of the type of initiating radicals released, ESR spin trapping experiments have been performed. Aryl radicals were trapped by PBN in **PTZ1** solution after 30 s of irradiation (Figure 14). Values of the hyperfine coupling constants for the radical adduct obtained were α_N = 14.3 G and α_H = 2.1 G which could be assigned to the aryl radical ($Ar^{\bullet}$), thus the fluorescence quenching of **PTZ1** in its first excited singlet state by Iod is confirmed, in agreement with the results obtained in the photopolymerization experiments.

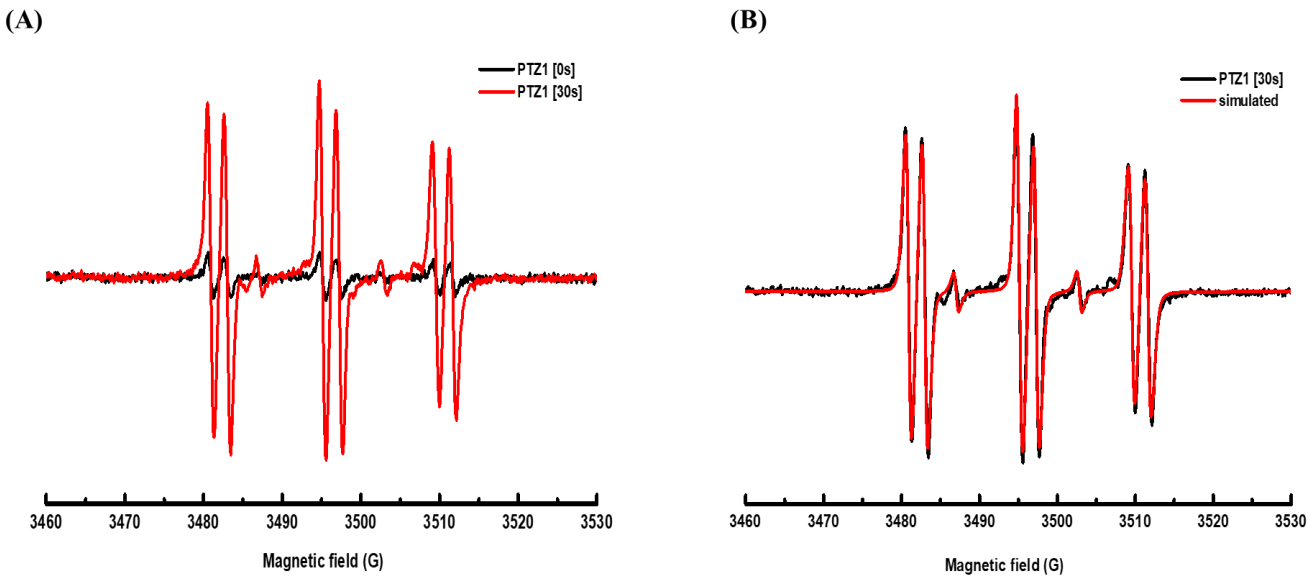

Figure 14. ESR spectra for **PTZ1**/Iod solution recorded in the presence of PBN and *tert*-butylbenzene with a LED@405nm: (A) before and after irradiation; (B) experimental and simulated spectra observed after irradiation (at t = 30 s).

Due to its high photoreactivity during the FRP of TA, the two-component system **PTZ3**/Iod (0.1%/1% w/w) was selected for 3D printing experiments upon laser diode irradiation at 405 nm. The 3D patterns denoted by "IS2M" shown in Figure 15 characterized by numerical optical microscopy have a great thickness (≈ 1400 µm), high spatial resolution, and require a very short irradiation time to be generated (15 s) which confirms the high photosensitivity of the system used (**PTZ3**/Iod).

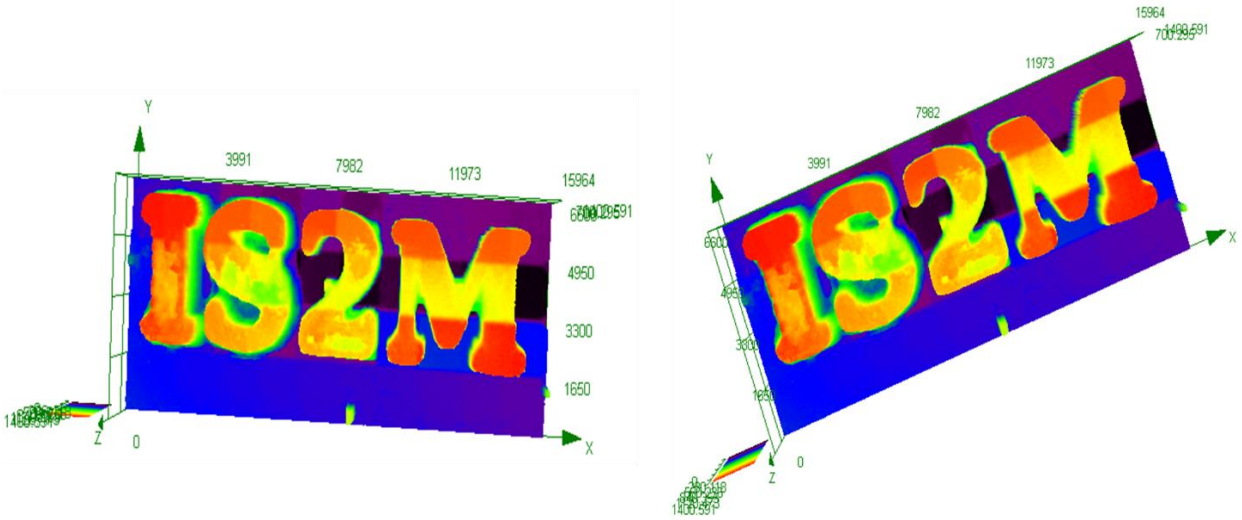

Figure 15. 3D patterns obtained upon exposure to a laser diode @405 nm characterized by numerical microscopy for compound **PTZ3** with Iod (0.1%/1% w/w) in TA.

4. Conclusion

In this article, three new photoinitiators based on the phenothiazine chromophore were successfully synthesized and used as Type I and two-component visible light photoinitiating systems. These compounds achieved high final conversions during the FRP of acrylate, the CP of epoxides, and during IPN synthesis upon irradiation using a LED@405 nm. Photoinitiation mechanism for the mono-component systems was established by mean of the CO_2 detection tests, and during the ESR spin-trapping experiments. Conversely, photoinitiating mechanism occurring for two-component systems could be determined on the basis of fluorescence quenching experiments. Notably, photoinitiation ability of **PTZ3** allowed the fabrication of 3D objects by laser write and 3D printing technologies. In addition, the dual photo/thermal behavior of these

compounds have been also shown. Future developments of other Type I and Type II photoinitiators based on the phenothiazine scaffold that can be activated at longer wavelengths will be proposed in upcoming studies.

Acknowledgment

This work received funding by the CY Initiative of Excellence (grant "Investissements d'Avenir" ANR-16-IDEX-0008) and developed during Frédéric Dumur's stay at the CY Advanced Studies whose support is gratefully acknowledged. The authors want to thank also the Foundation Pierre et Jeanne SPIEGEL for the funding of this work (Adel Noon).

References

[1] M.A. Tehfe, F. Louradour, J. Lalevée, and J.P. Fouassier, Photopolymerization reactions: On the way to a green and sustainable chemistry, *Applied Sciences*, 2013, **3**(2), 490-514.

[2] G. Yilmaz, S. Beyazit, and Y. Yagci, Visible light induced free radical promoted cationic polymerization using thioxanthone derivatives, *Journal of Polymer Science Part A: Polymer Chemistry*, 2011, **49**(7), 1591-1596.

[3] J. Stansbury, and W. Jeffrey, Curing dental resins and composites by photopolymerization, *Journal of esthetic and restorative dentistry*, 2000, **12**(6), 300-308.

[4] B. Baroli, Photopolymerization of biomaterials: issues and potentialities in drug delivery, tissue engineering, and cell encapsulation applications, *Journal of Chemical Technology & Biotechnology: International Research in Process, Environmental & Clean Technology*, 2006, **81**(4), 491-499.

[5] H. Yang, G. Li, J.W. Stansbury, X. Zhu, X. Wang, and J. Nie, Smart antibacterial surface made by photopolymerization, *ACS Applied Materials & Interfaces*, 2016, **8**(41), 28047-28054.

[6] K. Song, M. Mohseni, and F.Taghipour, Application of ultraviolet light-emitting diodes (UV-LEDs) for water disinfection: A review, *Water research*, 2016, **94**, 341-349.

[7] K.D. Jandt, R.W. Mills, G.B. Blackwell, and S.H. Ashworth, Depth of cure and compressive strength of dental composites cured with blue light emitting diodes (LEDs), *Dental Materials*, 2000, **16**(1), 41-47.

[8] G. La Torre, L. Marigo, G.A. Pascarella, and G. Rumi, Light-emitting diodes (LED) technology applied to the photopolymerization of resin composites, *Minerva Stomatologica*, 2003, **52**(5), 193-200.

[9] N. Awwad, A.T. Bui, E.O. Danilov, and F.N. Castellano, Visible-light-initiated free-radical polymerization by homomolecular triplet-triplet annihilation, *Chem*, 2020, **6**(11), 3071-3085.

[10] J.P. Fouassier, and J. Lalevée, Photoinitiators for polymer synthesis: scope, reactivity, and efficiency, *John Wiley & Sons*, 2012.

[11] K. Sun, Y. Xu, F. Dumur, F.Morlet-Savary, H. Chen, C. Dietlin, B. Graff, J. Lalevée, and P. Xiao, In silico rational design by molecular modeling of new ketones as photoinitiators in three-component photoinitiating systems: application in 3D printing, *Polymer Chemistry*, 2020, **11**(12), 2230-2242.

[12] H. Mokbel, D. Anderson, R. Plenderleith, C. Dietlin, F. Morlet-Savary, F. Dumur, D. Gigmes, J.P. Fouassier, and J. Lalevée, Copper photoredox catalyst "G1": A new high performance photoinitiator for near-UV and visible LEDs, *Polymer Chemistry*, 2017, **8**(36), 5580-5592.

[13] A. Al Mousawi, A. Kermagoret, D.L. Versace, J. Toufaily, T. Hamieh, B. Graff, F. Dumur, D. Gigmes, J.P. Fouassier, and J. Lalevée, Copper photoredox catalysts for polymerization upon

near UV or visible light: Structure/reactivity/efficiency relationships and use in LED projector 3D printing resins, *Polymer Chemistry*, 2017, **8**(3), 568-580.

[14] Z. Li., X. Zou, G. Zhu, X. Liu, and R. Liu, Coumarin-based oxime esters: photobleachable and versatile unimolecular initiators for acrylate and thiol-based click photopolymerization under visible light-emitting diode light irradiation, *ACS applied materials & interfaces*, 2018, **10**(18), 16113-16123.

[15] D.E. Fast, A. Lauer, J.P. Menzel, A.M. Kelterer, G. Gescheidt, and C. Barner-Kowollik, Wavelength-dependent photochemistry of oxime ester photoinitiators, *Macromolecules*, 2017, **50**(5), 1815-1823.

[16] R. Zhou, H. Pan, D. Wan, J.P. Malval, and M. Jin, Bicarbazole-based oxime esters as novel efficient photoinitiators for photopolymerization under UV-Vis LEDs, *Progress in Organic Coatings*, 2021, **157**, 106306.

[17] W. Qiu, P. Hu, J. Zhu, R. Liu, Z. Li, Z. Hu, Q. Chen, K. Dietliker, and R. Liska, Cleavable unimolecular photoinitiators based on oxime-ester chemistry for two-photon three-dimensional printing, *ChemPhotoChem*, 2019, **3**(11), 1090-1094.

[18] J.T. Offenloch, E. Blasco, S. Bastian, C. Barner-Kowollik, and H. Mutlu, Self-reporting visible light-induced polymer chain collapse, *Polymer Chemistry*, 2019, **10**(33), 4513-4518.

[19] S. Chen, M. Jin, J.P. Malval, J. Fu, F. Morlet-Savary, H. Pan, and D. Wan, Substituted stilbene-based oxime esters used as highly reactive wavelength-dependent photoinitiators for LED photopolymerization, *Polymer Chemistry*, 2019, **10**(48), 6609-6621.

[20] Z.H. Lee, F. Hammoud, A. Hijazi, B. Graff, J. Lalevée, and Y.C. Chen, Synthesis and free radical photopolymerization of triphenylamine-based oxime ester photoinitiators, *Polymer Chemistry*, 2021, **12**(9), 1286-97.

[21] F. Hammoud, N. Giacoletto, G. Noirbent, B. Graff, A. Hijazi, M. Nechab, D. Gigmes, F. Dumur, and J. Lalevée, Substituent effects on the photoinitiation ability of coumarin-based oxime-ester photoinitiators for free radical photopolymerization, *Materials Chemistry Frontiers*, 2021, **5**(24), 8361-70.

[22] S. Liu, B. Graff, P. Xiao, F. Dumur, and J. Lalevée, Nitro-Carbazole Based Oxime Esters as Dual Photo/Thermal Initiators for 3D Printing and Composite Preparation, *Macromolecular Rapid Communications*, 2021, **42**(15), 2100207.

[23] F. Dumur, Recent advances on anthracene-based photoinitiators of polymerization, *European Polymer Journal*, 2022, **18**, 111139.

[24] F. Dumur, Recent advances on pyrene-based photoinitiators of polymerization, *European Polymer Journal*, 2020, **126**, 109564.

[25] M. Rahal, M. Abdallah, T.T. Bui, F. Goubard, B. Graff, F. Dumur, J. Toufaily, T. Hamieh, and J. Lalevée, Design of new phenothiazine derivatives as visible light photoinitiators, *Polymer Chemistry*, 2020, **11**(19), 3349-59.

[26] K. Pluta, B. Morak-Mlodawska, and M. Jeleń, Recent progress in biological activities of synthesized phenothiazines, *European journal of medicinal chemistry*, 2011, **46**(8), 3179-89.

[27] R. Guo, Y. Wang, Z. Huang, Q. Zhang, S. Xiang, S. Ye, W. Liu, and L. Wang, Phenothiazine dioxide-containing derivatives as efficient hosts for blue, green and yellow thermally activated delayed fluorescence OLEDs, *Journal of Materials Chemistry*, 2020, **8**(11), 3705-14.

[28] Z. Gomurashvili, and J.V. Crivello, Monomeric and polymeric phenothiazine photosensitizers for photoinitiated cationic polymerization, *Macromolecules*, 2002, **35**(8), 2962-9.

[29] M.R. Rodrigues, and M.G. Neumann, Cationic photopolymerization of tetrahydrofuran: A mechanistic study on the use of a sulfonium salt–phenothiazine initiation system, *Journal of Polymer Science Part A: Polymer Chemistry*, 2001, **39**(1), 46-55.

[30] P. Chao, R. Gu, X. Ma, T. Wang, and Y. Zhao, Thiophene-substituted phenothiazine-based photosensitisers for radical and cationic photopolymerization reactions under visible laser beams (405 and 455 nm), *Polymer Chemistry*, 2016, **7**(32), 5147-56.

[31] X. Ma, R. Gu, L. Yu, W. Han, J. Li, X. Li, and T. Wang, Conjugated phenothiazine oxime esters as free radical photoinitiators, *Polymer Chemistry*, 2017, **8**(39), 6134-42.

[32] M. Abdallah, T.T. Bui, F. Goubard, D. Theodosopoulou, F. Dumur, A. Hijazi, J.P. Fouassier, and J. Lalevée, Phenothiazine derivatives as photoredox catalysts for cationic and radical photosensitive resins for 3D printing technology and photocomposite synthesis, *Polymer Chemistry*, 2019, **10**(45), 6145-56.

[33] J.B. Foresman and A. Frisch, Exploring chemistry with electronic structure methods, *Gaussian Inc., Pittsburgh*, PA, 2nd edn, 1996.

[34] M.J. Frisch, G.W. Trucks, H.B. Schlegel, G. E. Scuseria, M.A. Robb, J. R. Cheeseman, V.G. Zakrzewski, J.A. Montgomery, J.R.E. Stratmann, J.C. Burant, S. Dapprich, J.M. Millam, A.D. Daniels, K.N. Kudin, M.C. Strain, O. Farkas, J. Tomasi, V. Barone, M. Cossi, R. Cammi, B. Mennucci, C. Pomelli, C. Adamo, S. Clifford, J. Ochterski, G.A. Petersson, P.Y. Ayala, Q. Cui, K. Morokuma, P. Salvador, J.J. Dannenberg, D.K. Malick, A.D. Rabuck, K. Raghavachari, J.B. Foresman, J. Cioslowski, J.V. Ortiz, A.G. Baboul, B.B. Stefanov,G. Liu, A. Liashenko, P. Piskorz, I. Komaromi, R. Gomperts, R.L. Martin, D.J. Fox, T. Keith, M.A. Al-Laham, C.Y. Peng, A. Nanayakkara, M. Challacombe, P.M.W. Gill,B. Johnson, W. Chen, W. M. Wong, J. L. Andres,C. Gonzalez, M. Head-Gordon, E.S. Replogle andJ. A. Pople, *Gaussian 03, Revision B-2, Gaussian Inc., Pittsburgh*, PA, 2003.

[35] X. Allonas, J.P. Fouassier, M. Kaji, and Y. Murakami, Excited state processes in a four-component photosensitive system based on a bisimidazole derivative, *Photochemical & Photobiological Sciences*, 2003, **2**(3), 224-9.

[36] J. Lalevée, N. Blanchard, M.A. Tehfe, F. Morlet-Savary, and J.P. Fouassier, Green bulb light source induced epoxy cationic polymerization under air using tris (2,2'-bipyridine) ruthenium (II) and silyl radicals, *Macromolecules (Print)*, 2010, **43**(24), 10191-5.

[37] J. Lalevée, N. Blanchard, M.A. Tehfe, M. Peter, F. Morlet-Savary, D. Gigmes, and J.P. Fouassier, Efficient dual radical/cationic photoinitiator under visible light: a new concept, *Polymer Chemistry*, 2011, **2**(9), 1986-91.

[38] M. Schmitt, S. Kuhn, M. Wotocek, and R. Hempelmann, Photo-curing of off-set printing inks by functionalized ZnO nanoparticles, *Zeitschrift für Physikalische Chemie*, 2011, **225**(3), 297-311.

[39] B. Kraeutler, C.D. Jaeger, and A.J. Bard, Direct observation of radical intermediates in the photo-Kolbe reaction-heterogeneous photocatalytic radical formation by electron spin resonance, *Journal of the American Chemical Society*, 1978, **100**(15), 4903-4905.

TOC graphic